

Design of Double-Pass Dispersion-Compensated Raman Amplifiers for Improved Efficiency: Guidelines and Optimizations

M. Tang, *Student Member, IEEE*, Y. D. Gong, and P. Shum, *Member, IEEE*

Abstract—In this paper, an intensive theoretical and experimental investigation is conducted on the dispersion-compensating Raman amplification module configured in double-pass geometry. An analytical model is developed to study the gain/pump efficiency improvement and the noise performance in a novel double-pass discrete-Raman-amplifier (DCRA) system. This paper demonstrates that the gain and pump efficiency can be improved significantly by using the double-pass configuration and the pump light reflector. The impairments of multipath-interference (MPI) noise due to the Rayleigh scattering and the external reflection are analyzed in order to balance the high gain efficiency and the enhanced MPI noise in the double-pass DCRA. Furthermore, the nonlinear penalty in the DCRA system is investigated and a 10-Gb/s nonreturn-to-zero (NRZ) signal transmission in a 4×100 -km fiber system is simulated. The signal quality and bit-error rate are examined, and the optimization is done with reference to the input signal level and Raman gain; hence, the impact of double-pass DCRA on the dispersion-compensated optical communication systems is explored.

Index Terms—Discrete Raman amplifier (DCRA), double-pass, fiber nonlinearity, multipath interference (MPI), optical fiber amplifiers, Raman effects, Rayleigh scattering.

I. INTRODUCTION

IN RECENT years, the optical telecommunications industry has seen a unique explosion in growth largely driven by technology and massive increases in data-traffic bandwidth demand. To provide sufficient cost-efficient network capacity for future bandwidth demand, higher bit-rate and higher channel density systems are being rapidly developed. The discoveries in novel optical fiber amplifier devices especially enable the evolution of the optical network infrastructure [1]. Among the various competing candidates for next-generation optically amplified transmission systems, fiber Raman amplifiers (FRAs) with the distributed gain along fiber transmission lines offer the necessary low-noise amplification for economical field-deployed systems [2]–[4]. The Raman amplifier has been proven to be an effective amplifying device for providing relative flat gains over wide bandwidth in the *C* band (1530–1565 nm) and *L* bands (1565–1625 nm) [1] and is being deployed in almost

every new long-haul or ultralong-haul fiber-optic transmission systems, making it one of the widely used nonlinear optical devices in telecommunications [3].

Raman amplifiers can appear in a distributed, lumped, or discrete structure, or optionally in a hybrid amplifying structure when used in combination with erbium-doped fiber amplifiers (EDFAs). Discrete Raman amplifiers (DCRAs), mostly in the form of a pumped dispersion-compensating fiber (DCF), overcome the bandwidth limitations created by the discrete energy levels of erbium in EDFAs [3], [5]. Moreover, appropriately designed all-Raman systems combining distributed and discrete amplifiers could reduce numbers of discrete components compared with EDFA-based systems. The DCF is a particular convenient gain medium [6], as it can be used not only as a dispersion-compensating medium but as an amplifying medium with a Raman gain efficiency five to ten times larger than that of standard single-mode fibers (SSMFs) as well. By using a modest amount of pump power, the DCRA can be used to offset the loss of the dispersion compensation module and to extend new gain bandwidth such as *S* band (1480–1530 nm) or *U* band (1625–1675 nm).

However, there are two problems associated with DCF as an amplification medium. One is that the DCF length is fixed when it is used to compensate the dispersion of a specific fiber span. On the other hand, when the amplifier acts only as a discrete amplifier to open a new bandwidth window, rather than being used for dispersion compensation, the fiber length can only be adjustable within a limited range to avoid additional dispersion accumulation. Therefore, DCF is normally limited to be less than 10 km as an amplifying device. The short DCF length reduces the amount of available gain for a given pump power, thereby decreasing the pump efficiency. The high pump power needed for sufficient signal amplification increases the fiber nonlinearity and the system costs. At this power level (such as ~ 1 W), some fiber components such as connectors and wavelength-division-multiplexers (WDMs) are highly vulnerable to damage. Thus, an optimum gain distribution of amplifier must be found, and the improvements in pump efficiency are needed to make the DCRAs competitive with the performance of new types of EDFAs [7].

In this paper, the gain/pump efficiency improvement and the noise performance in a novel design of double-pass DCRA system, in which a narrow-band or wide-band reflector is used to retroreflect the signal or pump light, are investigated. Different geometries are discussed without additional expense of extra pump lasers. The system is evaluated with regard to the

Manuscript received February 1, 2004; revised May 18, 2004.

M. Tang and P. Shum are with the Network Technology Research Centre (NTRC), School of Electrical and Electronics Engineering, Nanyang Technological University, Singapore 637553, Singapore (e-mail: tangming@pmail.ntu.edu.sg).

Y. D. Gong is with the Institute for Infocomm Research, Innovation Center, Singapore 637723, Singapore.

Digital Object Identifier 10.1109/JLT.2004.832433

gain enhancement, noise figure, and fiber nonlinearity in comparison with the typical backward-pumping Raman amplifier. The requirement of components according to the performance optimization is also illustrated. Section II presents the novel DCRA design and the analytic model to describe the gain and noise performance considering the effect of signal/pump double-pass geometry. The multipath interference (MPI) noise due to the Rayleigh scattering and external reflection is discussed in detail. In addition, experiments are implemented to validate the modeling method and prove the feasibility of double-pass DCRA. Section III discusses the requirements of various components in this system, such as pump stability, fiber dispersion, and reflection ratio of reflector. In Section IV, the fiber nonlinear effect in this DCF-based double-pass DCRA is analyzed to compare the nonlinear impairments with the conventional counterpumped Raman amplifier. Further, the 10-Gb/s nonreturn-to-zero (NRZ) signal qualities in the transmission span employing double-pass DCRA are numerically studied. Bit-error rate (BER) performance related to the input signal power and Raman gain of DCRA is discussed to evaluate the impact of this device in practical optical communication system. Discussions and conclusions are given in Section V.

II. SYSTEM DESIGN AND SIMULATION MODEL

Fig. 1 shows the schematic of the double-pass DCRA used in theoretical analysis and experiments. The input signal from a tunable laser source (TLS) is injected into 3-km DCF through the optical circulator (OC) port 1. The dropped signal from the circulator copropagates with the pump power in the DCF and is reflected to counterpropagate with the pump. Both narrow-band fiber Bragg grating (FBG) and wide-band chirp-FBG (CFBG) (reflection ratio $R > 99\%$) can be used here as the reflector. In addition, the CFBG can provide a flexibility to compensate the dispersion of the fiber span dynamically [8]. Thus, the length of the gain medium is not restricted by the required amount of accumulated dispersion in transmission lines. Moreover, a wide-band reflector or FBG at pump wavelength can be deployed at the fiber end to reflect the residual part of the pump power to increase the gain efficiency further [9].

A. Raman Gain Characteristics With Small Pump Depletion

At the steady-state operating condition, there are four types of lightwaves traveling in the amplifier, which determine the gain profile: the forward signal, the forward pump, the reflected signal, and the reflected pump. The power evolution of lightwaves can be described by the following coupled equations [10]:

$$\pm \frac{dP_{SK}}{dz} = -\alpha_s P_{SK} + g \cdot P_{SK} P_{Pf} \quad (1)$$

$$\pm \frac{dP_{PK}}{dz} = -\alpha_P P_{PK} - g \cdot \sum P_{SK} \cdot P_{PK}. \quad (2)$$

Here, $P_{SK} = P_{Sf}$ or P_{Sb} is the forward or backward signal power, and $P_{PK} = P_{Pf}$ or P_{Pb} is the forward/backward pump power, respectively. α_s or α_P is the fiber loss at the signal or pump wavelength. z is the propagation distance from the fiber input and $g = g_0/A_{\text{eff}} \cdot K$ is the effective Raman gain coefficient where g_0 is the Raman gain coefficient between signal and pump, A_{eff} is the effective fiber area, and K is the polarization

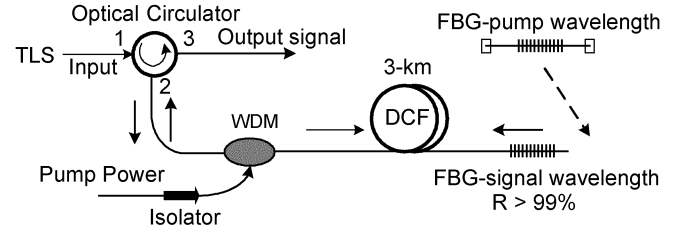


Fig. 1. Schematic system setup.

scrambling factor between pump and signal light. The temperature dependence is not considered because it is negligible [1]. The Rayleigh backscattering and amplified-spontaneous-emission (ASE)-induced system noise can be included additively (see hereafter).

In this double-pass system, by neglecting the pump depletion and using $P_{Pf}(L) = P_{Pb}(L)$, the pump power distribution $P_P(z)$ can be described as

$$\begin{aligned} P_P(z) &= P_{Pf}(z) + P_{Pb}(z) \\ &= P_{Pf}(0) \exp(-\alpha_P z) \\ &\quad + P_{Pb}(L) \exp[-\alpha_P(L-z)] \end{aligned} \quad (3)$$

where $P_{Pf}(0)$ is the input pump power, and $P_{Pb}(L) = P_{Pf}(0) \exp(-\alpha_P L)$. It is an equivalent bidirectional pumping scheme. Using the boundary condition $P_{Sf}(L) = P_{Sb}(L)$, the forward- and backward-transmission ON-OFF signal gain can be derived analytically as

$$\begin{aligned} G_{Rf}(z_1, z_2) &= \exp \left\{ \frac{g P_{Pf}(0) [\exp(-\alpha_P z_1) - \exp(-\alpha_P z_2)]}{\alpha_P} \right\} \\ &\quad \cdot \exp \left\{ \frac{g P_{Pb}(L) [\exp(\alpha_P(z_2 - L)) - \exp(\alpha_P(z_1 - L))]}{\alpha_P} \right\} \end{aligned} \quad (4)$$

$$\begin{aligned} G_{Rb}(z_1, z_2) &= \exp \left\{ \frac{g P_{Pf}(0) [\exp(\alpha_P(z_2 - L)) - \exp(\alpha_P(z_1 - L))]}{\alpha_P} \right\} \\ &\quad \cdot \exp \left\{ \frac{g P_{Pb}(L) [\exp(-\alpha_P z_1) - \exp(-\alpha_P z_2)]}{\alpha_P} \right\} \end{aligned} \quad (5)$$

where L is total fiber length. Thus, the output signal will experience the total ON-OFF Raman gain of $G_{Rf}(0, L) \cdot G_{Rb}(0, L)$ (note that $G_{Rb}(z_1, z_2)$ is the Raman gain experienced from z_2 to z_1).

B. ASE Noise Characteristics

With the same notation, the ASE noise spectral density in each state of polarization of a double-pass system can be described as $\pm dN_{SK}^{\text{ASE}}/dz = -\alpha_s N_{SK}^{\text{ASE}} + g \cdot (N_{SK}^{\text{ASE}} + hv) \cdot P_{Pf}$. Using the Raman gain (4), (5), the backward and forward ASE noise spectral density can be obtained, as follows:

$$\begin{aligned} N_{Sb}^{\text{ASE}}(z) &= N_{Sf}^{\text{ASE}}(L) A(0, L) G_{Rb}(0, L) + hv \\ &\quad \times \int_0^{L-z} g [P_{Pb}(L) \exp(-\alpha_P x) + P_{Pf}(0) \exp(-\alpha_P(L-x))] \\ &\quad \cdot A(0, x) G_{Rb}(L-x, L) dx \end{aligned} \quad (6)$$

$$\begin{aligned}
& N_{Sf}^{ASE}(L) \\
&= hv \int_0^L g [P_{Pf}(0) \exp(-\alpha_P x) + P_{Pb}(L) \exp(-\alpha_P(L-x))] \\
&\quad \cdot A(x, L) G_{Rf}(x, L) dx \quad (7)
\end{aligned}$$

where $A(z_1, z_2) = \exp[-\alpha_S(z_2 - z_1)]$ is the passive fiber loss; thus, the forward net gain G_f from distance z_1 to z_2 is $A(z_1, z_2)G_{Rf}(z_1, z_2)$, and the backward net gain G_b from distance z_2 to z_1 is $A(z_1, z_2)G_{Rb}(z_1, z_2)$.

C. MPI Noises Induced by the Rayleigh Scattering

Unlike the white noise random process feature of ASE, the MPI noises induced by Rayleigh backscattering are distributed over the same wavelength band of the transmitted signal, which is generated by the beating of multiple differently delayed replicas of the signal itself. The contribution from signal-MPI beat noise is more serious in our system with the introduction of external reflection. We will examine the Rayleigh-backscattered (RB) and double-Rayleigh-backscattered (DRB) light of forward- and backward-propagating signals. The flows of signal and RB/DRB light are shown in Fig. 2. We derive the RB and DRB noise power separately as

$$P_{Sf}^{RB}(0) = rP_{Sf}(0)G_b(0, L) \int_0^L \frac{G_f(0, z)}{G_b(z, L)} dz \quad (8)$$

$$\begin{aligned}
P_{Sf}^{DRB}(L) &= r^2 P_{Sf}(0) G_f(0, L) \\
&\quad \times \int_0^L \frac{1}{G_f^2(0, z)} \int_z^L G_f^2(0, x) dx \cdot dz \quad (9)
\end{aligned}$$

$$P_{Sb}^{RB}(L) = rP_{Sb}(L)G_f(0, L) \int_0^L \frac{G_b(z, L)}{G_f(0, z)} dz \quad (10)$$

$$\begin{aligned}
P_{Sb}^{DRB}(0) &= r^2 P_{Sb}(L) G_b(0, L) \\
&\quad \times \int_0^L \frac{1}{G_b^2(z, L)} \int_z^L G_b^2(x, L) dx \cdot dz \quad (11)
\end{aligned}$$

where $P_{Sb}(L) = P_{Sf}(L) = P_{Sf}(0)G_f(0, L)$, G_f and G_b are net gains, and r is the Rayleigh-backscattering coefficient. Since the Rayleigh scattering of light occurs continuously in fibers, $P_{Sb}^{RB}(L)$ and $P_{Sf}^{DRB}(L)$ will be reflected by the FBG and experience the Raman gain. Considering all these factors, we can obtain a general expression of noise figure (NF) of the double-pass DCRA in which ASE and MPI noises are generated simultaneously. In the beat-noise-limited detection, one can write the effective NF of DCRA [11] as

$$\text{NF} = \frac{1}{G_{\text{ON-OFF}}} \left[\frac{2N_{Sb}^{ASE}(0)}{hv} + \frac{\left(\frac{5}{9}\right) P_{\text{RB}}(0)}{hv \left(B_c^2 + \frac{B_s^2}{2}\right)^{\frac{1}{2}}} + 1 \right]. \quad (12)$$

Here $G_{\text{ON-OFF}}$ is the overall ON-OFF Raman gain, and $P_{\text{RB}}(0)$ is the total MPI noise at the output port. Notice that ASE light is randomly polarized but the degree of polarization of RB light

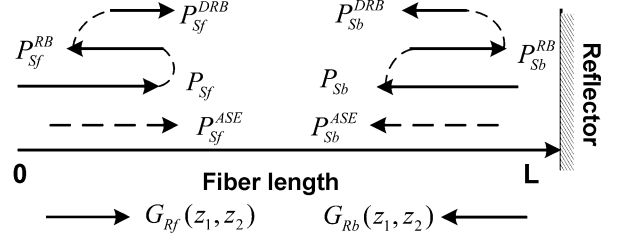


Fig. 2. Signal and noise (ASE and MPI) flows.

is 5/9. If we replace the ON-OFF gain $G_{\text{ON-OFF}}$ by the net gain $G = G_f \cdot G_b = G_{\text{ON-OFF}} \exp(-2\alpha_S L)$, which includes the transmission loss, (12) represents the real total NF of the amplification system.

D. Theoretical and Experimental Results

The double-pass DCRA is designed to cost effectively compensate the dispersion and loss of conventional single-mode fiber (SMF) or nonzero-dispersion fiber (NZDF). The parameters of different fiber types are listed in Table I. Nowadays, the transmission systems require amplifier spacing of at least 80 km in NZDF with five to six spans between electrical regeneration, while the span of standard telecommunication SMF is about 40–50 km. In double-pass geometry, the DCF length required for an 80-km NZDF span is less than 2 km, regardless of the use of CFBG. It is well known that the effective length of pump L_{eff} determines the effective fiber length for the Raman interaction and is defined as $[1 - \exp(-\alpha_P L)]/\alpha_P$. Since the length of DCF is quite short, the pump reflector is certainly needed to increase the effective Raman interaction length and improve the gain efficiency. In order to compare with the experimental results, we design and implement the DCRA module to compensate the 40-km SMF span. A 3-km DCF is needed in the double-pass scheme, and the L_{eff} is about 2.4 km.

If the input light power of a signal at 1554 nm in SMF is -10 dBm, after transmission in SMF, the input signal power in DCF is -17.2 dBm. First, we analyzed the gain performance of double-pass DCRA without the pump reflector. A pump light downshifted 13.2 THz from the signal frequency was used to provide the maximum Raman gain. Fig. 3 shows the calculated signal and pump power distributions along the DCF for our double-pass configuration and the traditional single-pass backward-pumping amplifier. Both cases were simulated to provide the same net gain of 17.2 dB. The double-pass amplifier was pumped with 458 mW, and the backward-pumping single-pass amplifier was pumped with 848 mW. Clearly, the double-pass configuration achieved the same gain performance with 46% less pump power in the same fiber length. The normalized pump power transmitted in the single- and double-pass system (calculated by numerical simulation) is shown in Fig. 4. The pump power calculated by neglecting pump depletion in double-pass geometry is also plotted, which matches the numerical results very well. We can observe that although the gain efficiency is much higher in the double-pass system, a significant fraction of pump power exits at the end of DCF. The fact that there is more than 60% of unused pump power in the 3-km double-pass system suggests that the gain efficiency could be improved by adding a pump light reflector.

TABLE I
PARAMETERS OF DIFFERENT FIBER TYPES

Parameter	α @1550	D@1550	n_2/A_{eff}	r	g_0/A_{eff}
Fiber type	nm [dB/km]	nm [ps/km/nm]	$[W^{-1}]$	$[km^{-1}]$	$[1/W/km]$
SMF	0.18	+16.3	—	—	0.37
DCF	0.49	-102	14.5×10^{-10}	2.7×10^{-4}	3.40
NZDF	0.22	+4.4	—	—	—

α : attenuation loss, D: dispersion, r : Rayleigh backscattering coefficient, g_0/A_{eff} : Raman gain

coefficient for 1455 nm pumping, n_2/A_{eff} : nonlinear coefficient, where n_2 is the nonlinear

refractive index.

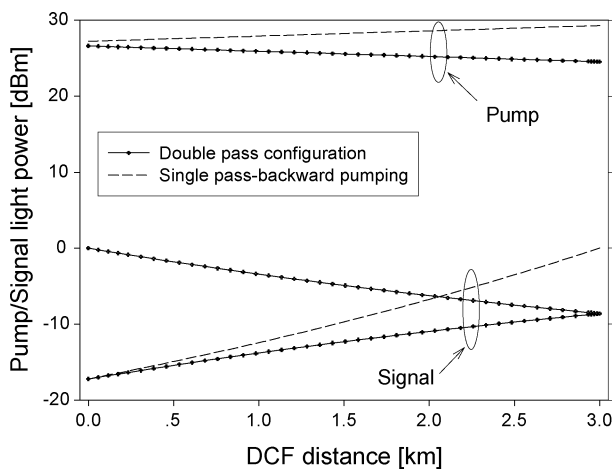


Fig. 3. Signal and pump power distributions along the 3-km DCF for double- and single-pass schemes.

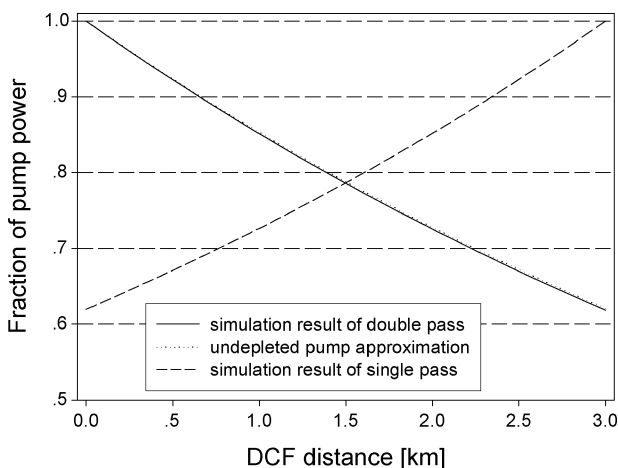


Fig. 4. Normalized pump power distribution along the amplifier fiber for single- and double-pass system. Simulation and analytical results are compared for double-pass system.

We then calculated the gain of the double-pass DCRA with the pump reflector using the theoretical models (3) to

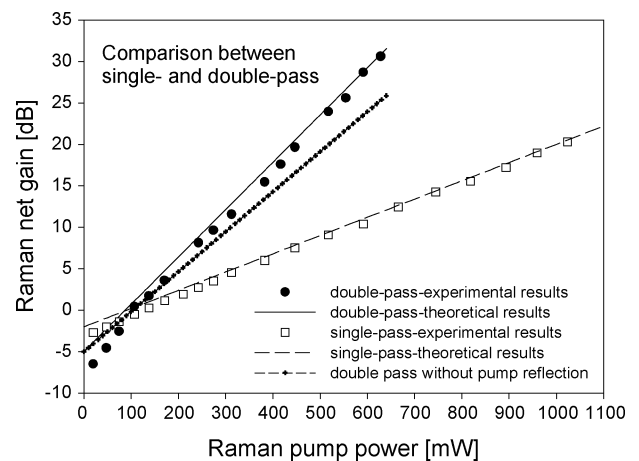


Fig. 5. Comparison of Raman net gains in single- and double-pass system.

(5) and evaluated the results in experiments. The experiment configuration implemented is illustrated in Fig. 1. A 1455-nm Raman fiber laser (RFL) with relative intensity noise (RIN) < -124 dB/Hz was employed as the continuous-wave (CW) Raman pump source and was injected through a WDM. The measured 3-dB gain bandwidth of this pump was 20 nm, and the peak Raman gain wavelength is 1554 nm. The FBGs were replaced by a wide-band reflector (reflectivity $> 90\%$ from 1260 to 1650 nm) to simplify the setup. It is worth noting that the average total polarization-mode dispersion (PMD) value of our DCF is measured as 0.82 ps, which is high enough to neglect the polarization dependence of the Raman gain [12], and it is reasonable to avoid the depolarization of the pump source. In Fig. 5, Raman net gains in the same 3-km DCF were plotted for the single- and double-pass system with the pump reflector. The net gain of the double-pass system without the pump reflector was also plotted for comparison. The insertion loss caused by the reflector and the connector were taken into account. The input signal condition was the same as that in Fig. 3. With the pump reflection, a 3~5-dB gain increase was obtained when the pump power exceeded 300 mW in the double-pass geometry. Our theoretical model presented a good prediction of the gain performance, especially at the high-gain

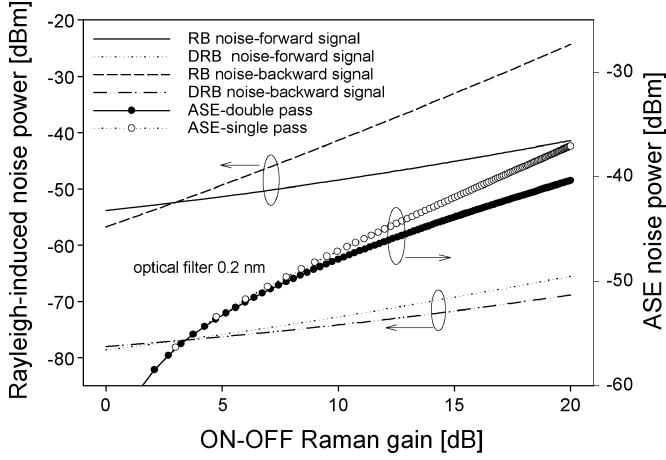


Fig. 6. ASE and RB/DRB noise power versus Raman gain of double-pass DCRA. Input signal: -17.2 dBm at 1554 nm.

region, and the double-pass amplifier exhibited much higher gain efficiency compared with the typical single-pass amplifier. Due to the considerable pump depletion, there were relatively large discrepancies between the theoretical and experimental results when the pump power was less than 100 mW in the double-pass DCRA.

In order to evaluate the noise performance of the double-pass system, we plotted the ASE and all of the RB/DRB noise powers versus Raman gain in Fig. 6. The input signal condition was assumed to be the same as that in Fig. 3. The ASE noise power was integrated within the optical filter bandwidth of 0.2 nm. For comparison, we also plotted the ASE noise power of a traditional backward-pumped 6 -km DCF single-pass system. It was clear that the ASE noise in our double-pass system was suppressed by the equivalent bidirectional pumping scheme. However, the MPI noises due to the reflection played an important role in the double-pass system. As shown here, the double-RB light was quite weak because of the short fiber length and very low input signal power. However, the RB light of the signal induced by the reflection of the FBG was a key component when considering the noise performance. The output RB noise of the forward signal $P_{S_f}^{RB}(0)$ in (8) is of the same order as ASE, but the output RB noise of the backward signal $P_{S_b}^{RB}(0)$ in (10) increases with the Raman gain rapidly and overwhelms ASE power at the high-gain region. That is, the MPI noise is the main limitation factor of the double-pass Raman amplifier. We compare the total NF performance versus Raman ON-OFF gain with and without considering MPI noise contribution in Fig. 7. When calculating the NF, we use the optical signal bandwidth $B_S = 10$ GHz and the receiver electrical bandwidth $B_e = 10$ GHz [13]. In general, the NF can be reduced with the increasing distributed Raman gain, which fits to the curve of ASE-induced NF in Fig. 7. However, unlike the NF in traditional DCRA, the NF in the double-pass system increases drastically due to the MPI impairments when the Raman gain exceeds 14 dB, limiting the high-gain usage of the double-pass DCRA. Although the total NF is less than 8.5 dB at the 20 -dB Raman gain, the tradeoff between the pump gain efficiency and NF tolerance must be taken into consideration according to the system requirements.

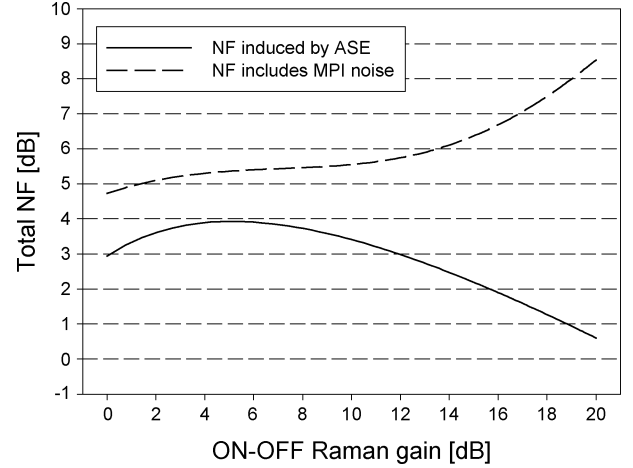


Fig. 7. Total NF with/without considering the MPI noise.

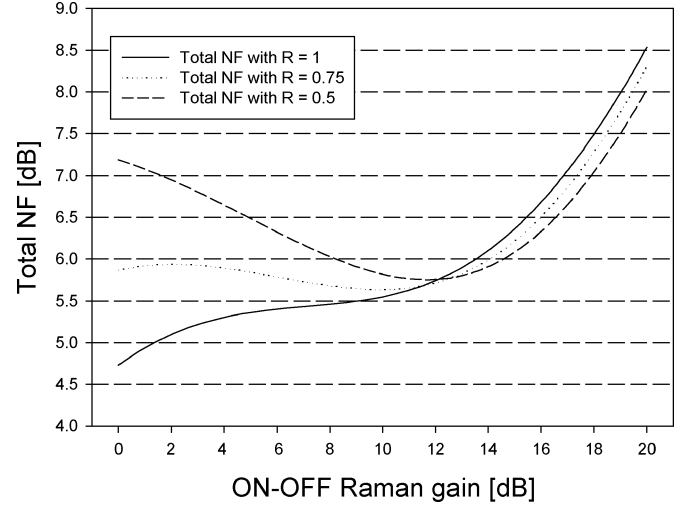


Fig. 8. Total NF with different reflection ratio (R) of signal reflector.

III. DESIGN ISSUES OF DOUBLE-PASS DCRA

This section discusses the design issues of some key components in the double-pass systems. Requirements and conditions that complied with the system performances are specified to make the double-pass DCRA a practical and feasible amplifier module.

A. Optimization of the Signal Reflector

Since most of the Rayleigh-backscattering-induced noise is due to the RB light of the backward-propagating signal (shown in Fig. 6), we can try to vary the reflection ratio of FBG to control the reflected power of the backward amplified signal and, hence, reduce the total NF in the high-gain region. The tunable FBGs provide more flexibility to control the dispersion and net gain of the double-pass DCRA module. Fig. 8 shows the total NF for the reflection ratio of $R = 1$, 0.75 , and 0.5 of FBG, respectively. The lower the reflection ratio, the higher the NF at the zero gain operating point due to the additional insertion loss of FBG. By increasing the pump power and, consequently, the ON-OFF Raman gain, we observed the NF reduction in the high-gain region, and, hence, the minimum NF can be achieved at the higher gain. The minimum NF of $R = 0.75$ or 0.5 can

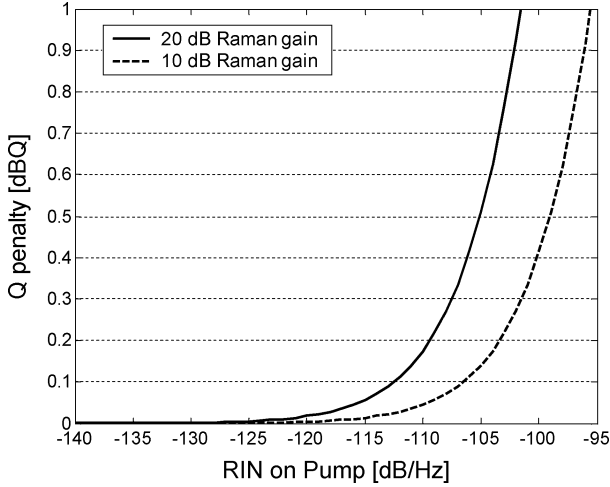


Fig. 9. Estimated Q penalty for different values of pump RIN at the copumping situation.

be obtained when the DRA is operating at the ON-OFF gain of 11 or 13 dB. It is clear that we can achieve less NF and higher Raman gain simultaneously by reducing the reflection ratio of FBG. Note that the required pump power in this case increases as well (such as the input pump power at $R = 0.5$ is 15% larger than that at $R = 1$). Indeed, if we set $R = 0$, which indicates the absence of a reflector, the signal will be received at the reflector end, and the DRA is a typical single-pass amplifier system. The RB noise has no effect on the system noise performance, but the advantages of double-gain and high pump efficiency are sacrificed.

B. Pump-RIN Transfer

Traditionally, Raman amplifiers are operated in the backward pumping geometry to minimize the pump-to-signal crosstalk and polarization-dependent gain. However, with the available low-noise pump sources, the copumping and bidirectional pumping schemes are feasible in practice [14]. Because there is a certain amount of copumping in our double-pass DCRA, it is important to consider the effects of pump-to-signal RIN transfer. Although the counterpumping scheme has a larger tolerance of pump RIN compared with the copumping scheme, the chromatic dispersion in the fiber causes the signal and pump wavelength to “walk off” and average the noise transfer from pump to signal. Analysis shows that fibers with high dispersion between the signal and pump wavelengths present a greater potential for the use in copumped Raman-amplified systems [15]. We follow the analysis procedures in [15] to study the performance degradation due to RIN transfer in copropagating Raman pump using the parameters listed in Table I and obtain the estimated quality (Q -factor) penalty in our DCF with varying Raman gain. The results are presented in Fig. 9. The copumped Raman amplification can tolerate up to -112 dB/Hz without suffering a 0.1-dB Q penalty with 20-dB Raman gain, and the double-pass DCRA can be made feasible using the pump sources with $RIN < -112$ dB/Hz. Thus, it is suitable to use our pump source ($RIN \leq -124$ dB/Hz) in this double-pass geometry with respect to system performances.

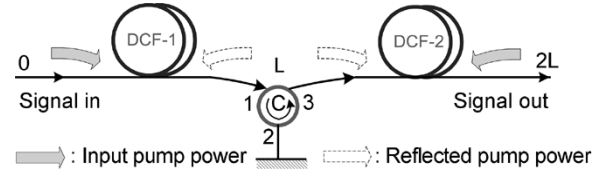


Fig. 10. Equivalent light path of double-pass DCRA.

IV. NONLINEAR IMPAIRMENTS IN DOUBLE-PASS DCRA

The double-pass DCRA has been proven to outperform the conventional counterpumped DCRA in the gain efficiency. The decrease of pump power requirements is extremely meaningful to make the Raman amplification competitive with the performance of EDFAs and recent thulium-doped fiber amplifiers (TDFAs) [16]. However, nonlinear impairments can occur for relatively high signal powers in DCFs with a small-effective area, even inside rather short fibers (in our case, 3-km DCF). Interchannel effects such as four-wave mixing (FWM) or cross-phase modulation (XPM) are mitigated by the high local dispersion of the DCF, but self-phase modulation (SPM) can still lead to signal distortion. The integrated nonlinear phase of a signal power evolution $P_s(z)$ over a fiber segment of length L is given by $\phi(L) = \int_0^L \gamma(z)P_s(z)dz$, where $\gamma(z) = \omega n_2/cA_{\text{eff}}$ is the fiber nonlinear coefficient, and ω is the center angular frequency of signal [11], [17]. We assume that different signal power evolutions on a transmission fiber of given constant dispersion produces the same signal distortion if they have the same integrated nonlinear phase. Our double-pass DCRA can be viewed as a bidirectional-pumping amplifier with a signal propagation distance twice the fiber length. A fair comparison can be made between the double-pass DCRA and the typical backward-pumping DCRA with the same total dispersion experienced. Since $P_s(z) = P_s(0)G(0, z)$, where $G(0, z)$ is the net gain, the signal nonlinear phase accumulation in the double-pass system can be modeled using (3) to (5) in the equivalent light path illustrated in Fig. 10. Here, we define the $G(0, z) = \exp(-\alpha_{\text{eq}}z)$, where α_{eq} is the equivalent local loss-amplification factor, and it can be derived [17], [18] from

$$\alpha_{\text{eq}}(z) = \alpha_S - \{gP_{Pf}(0) \exp(-\alpha_P z) + gP_{Pb}(L) \cdot \exp[-\alpha_P(L-z)]\} \quad \dots z \in [0, L] \quad (13)$$

$$\alpha_{\text{eq}}(z) = \alpha_S - \{gP_{Pf}(0) \exp[-\alpha_P(L-z)] + gP_{Pb}(L) \exp(-\alpha_P z)\} \quad \dots z \in [L, 2L] \quad (14)$$

where the parameters are defined in Section II, and the equivalent local loss-amplification factor of typical backward-pumping DCRA can be given as [18]

$$\Gamma_{\text{eq}}(z) = \alpha_S - gP_P(2L) \cdot \exp[-\alpha_P(2L-z)] \quad (15)$$

where $P_P(2L) = \ln(G_{\text{ON-OFF}})/(gL_{\text{eff}})$ is the input pump power at the fiber output port that supplies the same gain as the

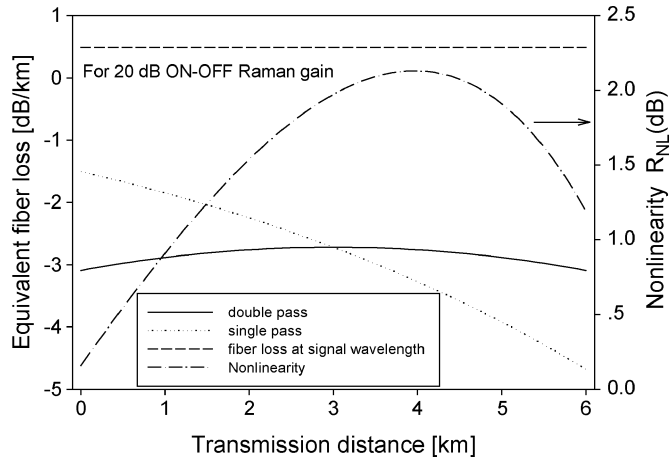


Fig. 11. Fiber equivalent loss of transmitted signal in double- and single-pass DCRA system with 20-dB ON-OFF Raman gain. The nonlinearity enhancement R_{NL} is plotted versus distance.

double-pass geometry. The calculated equivalent fiber loss-amplification factor of the double-pass DCRA is shown in Fig. 11, and the equivalent fiber loss of typical backward-pumping DCRA is plotted as well for comparison. It is evident that both amplifiers provide 20-dB ON-OFF gain. A flat distribution of Raman gain in the double-pass system is achieved. Since there is significant forward pumping in double-pass geometry, the fiber nonlinearity of this type of amplifier will be larger than that of the conventional counterpumped DCRA with the same input conditions. For the constant nonlinear impairments, we define R_{NL} to be the ratio of the overall nonlinear phase of the signal experienced in the double-pass DCRA relative to that experienced in the typical counterpumped DCRA

$$R_{NL}(2L) = \frac{\phi_{\text{double-pass}}(2L)}{\phi_{\text{backward}}(2L)} = \frac{\int_0^{2L} \exp[-\alpha_{\text{eq}}(z) \cdot z] dz}{\int_0^{2L} \exp[-\Gamma_{\text{eq}}(z) \cdot z] dz}. \quad (16)$$

The signal input power of the double-pass system should be $P_{\text{in}}/R_{NL}(2L)$, where P_{in} is the input power of conventional single-pass system, to insure the same cumulative nonlinearity. The R_{NL} as a function of transmission distance is plotted in Fig. 11. The initial increase of R_{NL} (in decibels) is due to the forward pumping, and the decrease near the fiber end is caused by the backward gain of counterpumping. Less than 1.5-dB power nonlinearity enhancements can be obtained in the double-pass DCRA with 20-dB ON-OFF gain (an approximately 17-dB net gain). This indicates the possibility to employ the double-pass DCRA as a preamplifier in a transmission system where the signal is attenuated during the transmission in span.

A comprehensive numerical simulation of the signal transmission characteristics in the fiber span employing double-pass DCRA is demonstrated in the following section. The system is considered as a cascade of four spans. In each span, the signal propagates in the 100-km SSMF span and acquires the loss and dispersion compensation in the DCRA module configured in double-pass geometry. An 8-km DCF is employed as the gain

medium, and the ideal dispersion and dispersion slope compensation is assumed. Pseudorandom-binary-sequence (PRBS) 64-b NRZ signals are assumed for intensity modulation at 10 Gb/s. The total signal envelope A propagated through the fiber span is modeled by the modified nonlinear Schrödinger equation (NLSE) [17]

$$j \frac{\partial A}{\partial z} - \frac{\beta_2}{2} \frac{\partial^2 A}{\partial T^2} - j \frac{\beta_3}{6} \frac{\partial^3 A}{\partial T^3} + \gamma |A|^2 A = -j \frac{\alpha}{2} \quad (17)$$

where β_2 is the group-velocity dispersion (GVD) coefficient, and β_3 is the third-order dispersion, respectively. The waveform evolutions can be obtained by numerically solving this equation with the split-step Fourier method (SSFM). Since the signal quality degradation caused by the pump depletion and RIN transfer is negligible according to the discussion in Section II and III, we can replace the attenuation coefficient α by the equivalent local loss-amplification factor α_{eq} defined in (13) and (14) to incorporate the Raman amplification [18]–[20]. We consider the effects of the double-pass DCRA on the single-channel signal transmission properties. The signal is output by means of a bandpass optical filter with a 3-dB bandwidth of 40 GHz and is then photodetected and filtered by a 12-GHz bandwidth low-pass electrical filter. The demodulated eye diagram can be obtained, and the BER can be estimated by following the steps in [18].

At the receiver, the signal and delayed signal will beat together; thus, the phase noise is converted into intensity noise by the incoherent mixing (since the Rayleigh-scattered pulse signal is produced along the long length of the amplifier cavity) [21]. In order to incorporate the MPI noise effect in the performance estimation, we study the electrical properties of Rayleigh-scattered light. Fig. 12 shows the electrical power spectrum of 10-Gb/s NRZ signals back to back, the signal after transmission, and the RB light, respectively, as measured by the electrical spectrum analyzer. The measured signal transmits through a 50-km SSMF span and is amplified by the counterpumped 3-km DCF, in which the 10-dB Raman gain is applied. The intensity noise of the Rayleigh component presents a wide-band white noise feature, and it has a similar power level with a transmitted signal component in the high-frequency region (above 40 GHz). This property suggests that a low-pass electrical filter would be necessary for the double-pass DCRA system, and we can include the MPI noise in the system by adding a wide-band electrical noise source at the receiver side.

The total loss in one span is about 26 dB (18 dB in the SMF, and 8 dB in the DCF). We calculate the BER and QQ factor with respect to the input signal mean power for transmission and present the results in Fig. 13, where Raman gains of different values are only applied in the double-pass DCRA. At low input power where ASE noise dominates, the performance is better with increasing input power, whereas it starts to degrade when the input power exceeds an optimum value, as a result of the fiber nonlinearity overwhelming the signal-to-noise ratio (SNR) improvement. For the error-free condition (BER of 10^{-12}), the power margin achieved by using double-pass DCRA is significant with the increasing Raman gain (an 8-dB power margin

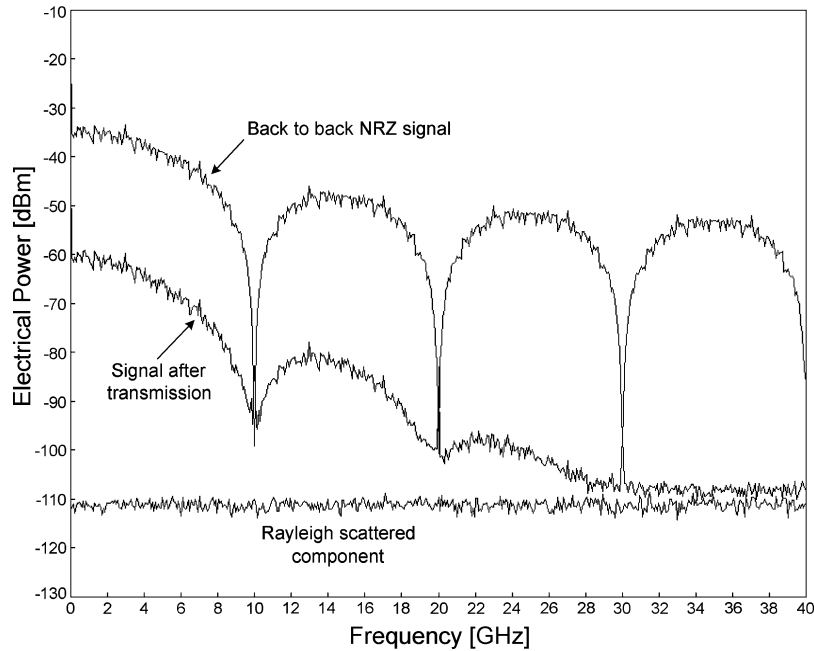


Fig. 12. Electrical power spectrum of three types of light: back-to-back 10-Gb/s NRZ signal source, signal after transmission, and Rayleigh-scattered signal light, respectively.

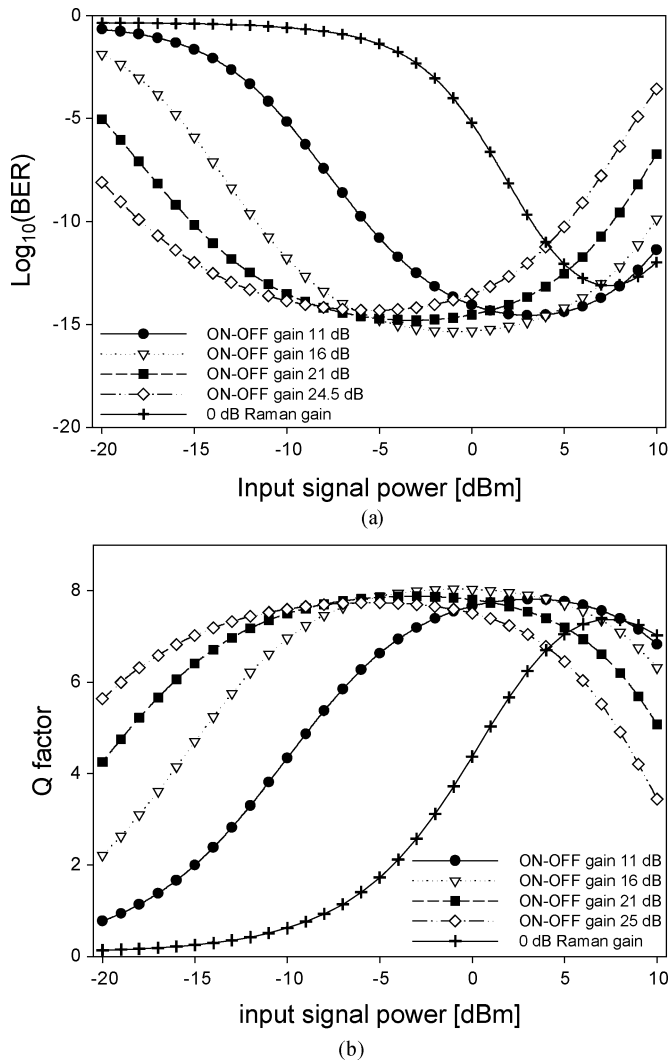


Fig. 13. (a) BER and (b) Q factor as a function of mean input signal power for the transmission span with different ON-OFF Raman gain in double-pass DCRA.

result can be obtained when an 11-dB Raman gain is applied). Furthermore, the minimal BER performance is obtained for a particular combination of input signal power and Raman gain (a 16-dB Raman gain and a 0-dBm input signal). Since the Raman amplification is provided only in the DCF module, the nonlinear penalty is mainly due to the SPM effects where high input power and high Raman gain are present. The degradation of BER performance at the high-Raman-gain regime is also due to the MPI noise because it is more strongly dependent on Raman gain and, hence, results in the noise floor [22]. The Rayleigh-scattered light is proportional to the transmitted signal power, and the enhanced MPI noise degrades the total noise performance at the high-power signal input condition, which should be avoided in the real applications.

In order to explore the optimal BER performance for the transmission span using the double-pass DCRA, we estimate the BER with respect to the input signal power in the span and the ON-OFF Raman gain in the DCRA. The contour map of calculated BER is plotted in Fig. 14. The best BER of the system can be achieved when the ON-OFF Raman gain in DCRA is 18 dB and the input signal power is 0 dBm. The corresponding input signal at the DCF is about -18 dBm to ensure a low-level MPI noise.

V. CONCLUSION

The DCFs are excellent gain mediums for DCRA because of high Raman gain efficiency due to a small effective area and high Ge concentration. Compared with the conventional discrete EDFAs, the DCRA can be used to develop an all-Raman-amplified system not limited to EDFA bands and to give additional flexibility to extend the available bandwidth. Since the cost/efficiency relation for Raman amplifiers is one of the major concerns for wide commercial use, the DCRA with a

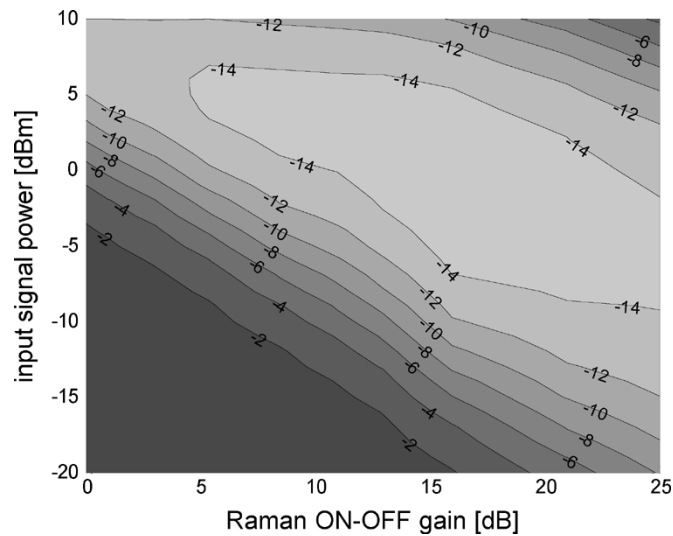


Fig. 14. Contour map of the $\log_{10}(\text{BER})$ as a function of the ON-OFF Raman gain in DCRA and the input signal power.

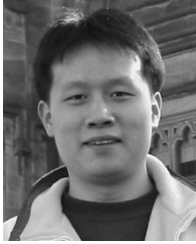
double-pass configuration to provide gain/pump efficiency improvement and acceptable noise performance was investigated. A theoretical model was developed for the transmitted signal, pump, and enhanced MPI noise due to the Rayleigh scattering and reflection in the double-pass system. Experiments were implemented by using a 3-km DCF to prove the feasibility of the proposed model. Both theoretical and experimental results represent significant enhancement in gain efficiency. With the appropriate FBG, in the same length of DCF, the double-pass DCRA generated the same net gain with 46% less pump power compared with the typical backward-pumped DCRA and achieved double dispersion compensation ability. For fixed dispersion compensation management, the double-pass geometry reduced the required DCF length/cost and made the gain distribution more evenly in the DCRA. With cascaded FBG or a wide-band reflector covering pump wavelength, a large amount of pump power was able to be reused and a 3 ~ 5-dB gain increase obtained with the same pumping conditions. It was also proven that MPI noise is the dominating source of noise impairments in the proposed double-pass DCRA system. From the NF performance, it can be seen that the MPI noise limits the usage of the proposed double-pass system in the very-high-gain regime. The tradeoff between high gain/efficiency and MPI noise impairments has been discussed with regard to the reflection ratio of the external reflector. The wideband white noise feature of MPI in the electrical domain suggests that a low-pass electrical filter should be needed to maintain the signal quality in transmission.

In order to evaluate the system transmission property with the noise and nonlinear impairments, a 4×100 -km SSMF span with double-pass DCRA has been simulated for a 10-Gb/s NRZ signal channel. The optimal performance is discussed according to the Raman gain and input signal power level. For large input power and high Raman gain, the quality penalty originates from both the nonlinear effect and the MPI noise. The compact, low-cost, high-efficient double-pass DCRA module is quite convenient for all-Raman-amplified dispersion-managed systems,

where low input power and moderate Raman gain in the DCRA are preferred to ensure the best signal quality.

REFERENCES

- [1] S. Namiki and Y. Emori, "Ultrabroad-band Raman amplifiers pumped and gain equalized by wavelength-division-multiplexed high-power laser diodes," *IEEE Select. Topics Quantum Electron.*, vol. 7, pp. 3–16, Jan./Feb. 2001.
- [2] A. Belahlou *et al.*, "Fiber design considerations for 40 Gb/s systems," *J. Lightwave Technol.*, vol. 20, pp. 2290–2305, Dec. 2002.
- [3] M. N. Islam, "Raman amplifiers for telecommunications," *IEEE J. Select. Topics Quantum Electron.*, vol. 8, May–June 2002.
- [4] F. D. Pasquale, F. Meli, E. Griseri, A. Sguazzotti, C. Tosetti, and F. Forghieri, "All-Raman transmission of 192 25-GHz spaced WDM channels at 10.66 Gb/s over 30×22 dB of TW-RS fiber," *IEEE Photon. Technol. Lett.*, vol. 15, pp. 314–316, Feb. 2003.
- [5] S. S. H. Yam, F. T. An, E. S. T. Hu, M. E. Marhic, T. Sakamoto, and L. G. Kazovsky, "Gain-clamped S-band discrete Raman amplifier," in *Tech. Dig. Optical Fiber Communication (OFC'02)*, 2002, pp. 385–387.
- [6] T. Miyamoto *et al.*, "Raman amplification over 100 nm-bandwidth with dispersion and dispersion slope compensation for conventional single mode fiber," in *Tech. Dig. Optical Fiber Communication Conf. (OFC'02)*, 2002, pp. 66–68.
- [7] A. K. Srivastava and Y. Sun, "Advances in erbium-doped fiber amplifiers," in *Optical Fiber Telecommunications, IVA*, I. P. Kaminow and T. Li, Eds. San Diego, CA: Academic, 2002, ch. 4.
- [8] T. Erdogan, "Fiber grating spectra," *J. Lightwave Technol.*, vol. 15, pp. 1277–1294, Aug. 1997.
- [9] J. W. Nicholson, "Dispersion compensating Raman amplifiers with pump reflectors for increased efficiency," *J. Lightwave Technol.*, vol. 21, pp. 1758–1762, Aug. 2003.
- [10] H. Kidorf, K. Rottwitz, M. Nissov, M. Ma, and E. Rabarjaona, "Pump interactions in a 100-nm bandwidth Raman amplifier," *IEEE Photon. Technol. Lett.*, vol. 11, pp. 530–532, May 1999.
- [11] R. J. Essiambre, P. Winzer, J. Bromage, and C. H. Kim, "Design of bidirectionally pumped fiber amplifiers generating double Rayleigh backscattering," *IEEE Photon. Technol. Lett.*, vol. 14, pp. 914–916, July 2002.
- [12] S. Popov, E. Vanin, and G. Jacobsen, "Influence of polarization mode dispersion value in dispersion-compensation fibers on the polarization dependence of Raman gain," *Opt. Lett.*, vol. 27, pp. 848–850, 2002.
- [13] R. Winzer, R. J. Essiambre, and J. Bromage, "Combined impact of double-Rayleigh backscatter and amplified spontaneous emission on receiver noise," in *Tech. Dig. Optical Fiber Communication Conf. (OFC'02)*, 2002, pp. 734–735.
- [14] F. D. Pasquale, F. Meli, E. Griseri, A. Sguazzotti, C. Tosetti, and F. Forghieri, "All-Raman transmission of 192 25-GHz spaced WDM channels at 10.66 Gb/s over 30×22 dB of TW-RS fiber," *IEEE Photon. Technol. Lett.*, vol. 15, pp. 314–316, Feb. 2003.
- [15] C. R. S. Fludger, V. Handerek, and R. J. Mears, "Pump to signal RIN transfer in Raman fiber amplifiers," *J. Lightwave Technol.*, vol. 19, pp. 1140–1148, Aug. 2001.
- [16] J. Bromage, H. J. Thiele, and L. E. Nelson, "Raman amplification is S-band," in *Tech. Dig. Optical Fiber Communication Conf. (OFC'02)*, 2002, pp. 383–385.
- [17] G. P. Agrawal, *Nonlinear Fiber Optics*, 3rd ed. San Diego, CA: Academic, 2001.
- [18] N. Takachio and H. Suzuki, "Application of Raman-distributed amplification to WDM transmission systems using 1.55- μm dispersion-shifted fiber," *J. Lightwave Technol.*, vol. 19, pp. 60–69, Jan. 2001.
- [19] A. Pizzinat, M. Santagiustina, and C. Schivo, "Impact of hybrid EDFA-distributed Raman amplification on a 4×40 -Gb/s WDM optical communication system," *IEEE Photon. Technol. Lett.*, vol. 15, pp. 341–343, Feb. 2003.
- [20] D. Dahan and G. Eisenstein, "Numerical comparison between distributed and discrete amplification in a point-to-point 40-Gb/s 40-WDM-based transmission system with three different modulation formats," *J. Lightwave Technol.*, vol. 20, pp. 379–388, Mar. 2002.
- [21] C. R. S. Fludger and R. Mears, "Electrical measurement of multipath interference in distributed Raman amplifiers," *J. Lightwave Technol.*, vol. 19, pp. 536–545, Apr. 2001.
- [22] S. A. E. Lewis, S. V. Chernikov, and J. R. Taylor, "Broadband high-gain dispersion compensating Raman amplifier," *IEEE Electron. Lett.*, vol. 36, pp. 1355–1356, 2000.



M. Tang (S'02) was born in China in May 1979. He received the B.Eng. degree in optoelectronics engineering from Huazhong University of Science & Technology (HUST), Wuhan, China, in 2001. He is currently working toward the Ph.D. degree in the Network Technology Research Centre (NTRC), School of Electrical and Electronic Engineering, Nanyang Technological University, Singapore.

His research interests are concerned with optical fiber communications, fiber Raman amplifiers/lasers, modeling of nonlinear fiber optical transmissions, and fiber-grating-based devices.

Y. D. Gong, photograph and biography not available at the time of publication.



P. Shum (M'96) received the B.Eng. and Ph.D. degrees in electronic and electrical engineering from of the University of Birmingham, Birmingham, U.K., in 1991 and 1995, respectively.

After receiving the degree, he became an honorary Postdoctoral Research Fellow with the University of Birmingham. In 1996, he conducted research in semiconductor laser and high-speed optical laser communication in the Department of Electrical and Electronic Engineering, Hong Kong University, as a Visiting Research Fellow. In July 1997, he joined the Department of Electronic Engineering, Optoelectronics Research Centre, City University of Hong Kong. In 1999, he joined the School of Electrical and Electronic Engineering, Nanyang Technological University, Singapore, and has been the Director of the Network Technology Research Centre since 2002. He has published more than 150 international journal and conference papers. His research interests are concerned with optical communications, nonlinear waveguide modeling, fiber gratings, and wavelength-division-multiplexing (WDM) communication systems.

Dr. Shum received the IEEE Electron Devices Society/Microwave Theory and Techniques Society (EDS/MTTS) India Chapter Best Paper Award for his paper in Photonics-98 in 1998, the Best Paper Award at the 3rd International Conference on Microwave and Millimeter Wave Technology, Beijing, China, in 2002, and the Singapore National Young Scientist Award in 2002 for his contribution on next-generation optical communication technologies.